Isoform-Specific Activation of p53B and p53C in Response to Nucleolar Stress in *Drosophila* wing imaginal discs

Andrea Vutera Cuda[1], Shivani Bajaj[1], Valeria Manara[1], and Paola Bellosta[1,2,*]

[1] Department of Cellular, Computational and Integrative Biology (CIBIO), University of Trento, Trento, TN 38123, Italy.

[2] Department of Medicine, NYU Langone Medical Center, New York, NY 10016, United States.

*Correspondence: paola.bellosta@unitn.it

Running title: p53 isoforms in response to nucleolar stress

Abstract

p53 isoforms remain poorly characterized despite recent evidence that they possess distinct functions in response to different cellular stresses. In *Drosophila*, four p53 isoforms are expressed from a single locus, but their individual roles under different stress conditions are not yet fully understood, partly due to limited tools for isoform-specific analysis. To address this gap, we developed and validated a set of isoform-specific qPCR primers that accurately distinguish all endogenous *Drosophila* p53 transcripts. Using this approach, we examined how each isoform responds to nucleolar stress, a mechanism triggered in humans by deregulation of ribosome biogenesis, often accompanied by increased p53 and apoptosis. In *Drosophila*, knockdown of *Nucleolar complex protein 1* (*NOC1*) impairs rRNA maturation and ribosomal assembly, triggering nucleolar stress and leading to upregulation of p53 level.

Using our isoform-specific qPCR primers, we found that p53B and the previously uncharacterized p53C isoforms are selectively upregulated in response to NOC1

knockdown, while p53A expression remains largely unaffected. This differential regulation underscores a stress-specific pattern of isoform activation distinct from the response typically observed under genotoxic stress conditions, where p53A predominates. These findings suggest the existence of isoform-specific roles in nucleolar stress signaling. Furthermore, our data support the possibility of autoregulatory interactions among p53 isoforms, whereby the stress-induced upregulation of one isoform may influence the transcriptional activity or stability of others. Notably, we also identified a previously unrecognized and evolutionarily conserved transcriptional response of p53 to nucleolar stress, which is detectable in both *Drosophila* and human systems. Together, these results highlight the significance of dissecting p53 isoform-specific functions to advance our understanding of cellular stress responses and their conservation across species.

Key words: p53 isoforms, nucleolar stress, NOC1, DNA damage, apoptosis, primer specificity, isoform primer design, *Drosophila.*

Introduction

Nucleolar stress is a cellular response to unbalanced ribosomal biogenesis (Boukoura and Larsen 2024). The nucleolus acts as a key stress sensor, responding to perturbations in ribosomal RNA (rRNA) processing and ribosome biogenesis by inducing the upregulation of p53 (Lindstrom et al. 2022).

Drosophila p53 shares significant structural and functional features with human p53 (Brodsky et al. 2000; Ingaramo et al. 2018; Ollmann et al. 2000). The *Dmp53* gene (FBgn0039044), herein referred to as *p53,* maps to chromosome 3R and encodes four mRNA isoforms (*p53A, p53B, p53C,* and *p53E*), which encode for three proteins predicted by the current deep RNA sequencing-based genome annotation (Boley et al. 2014). Indeed, p53A and p53C differ in their 5' untranslated regions (5'UTRs) but encode for the same open reading frame (ORF), resulting in an identical protein sequence of 44 KDa (Zhang et al. 2015; Chakravarti et al. 2022). This suggests that differential promoter regulation underlies their distinct functions in different cellular contexts. p53B is the longer

isoform, carrying a unique N-terminal domain and encoding for a 56 KDa protein. p53B is less studied, partly due to the lack of specific antibodies, and is considered the closest homolog to human p53 (Ingaramo et al. 2018). p53E is a shorter isoform predicted to encode a truncated protein of 38 KDa, lacking part of the N-terminal transactivation domain.

The most well-studied isoforms are *p53A* (FBtr0071021), also called ∆p53, and *p53B* (FBtr0071022), which reveal different regulation across developmental stages. Studies in eye discs, germline, and soma have shown that the *p53A* isoform is the most prevalent under physiological conditions and is necessary for the apoptotic response to ionizing radiation (Zhang et al. 2015; Chakravarti et al. 2022). *p53B* isoform is expressed at a much lower level than *p53A,* but is the major isoform responsible for inducing apoptosis upon activation of the pro-apoptotic gene *reaper* (*rpr*) and *head involution defective* (*hid*) activation (Zhang et al. 2015), whereas *p53A* is suggested to be involved in Apoptosis-induced proliferation (AiP), a mechanism in which the apoptotic cells secrete proliferative signals to the neighboring cells (Dichtel-Danjoy et al. 2013; Fogarty and Bergmann 2017).

One possible reason for these differential tissue-specific outputs is the competition among repressive and activating p53 isoforms, as *p53B* isoform acts primarily as a transactivator, whereas *p53A*, which is more broadly expressed across tissue types, acts both as a transactivator and transrepressor (Wylie et al. 2022). Indeed, in photoreceptor neurons, it was shown that cell death and survival decisions depend on antagonistic regulation of autophagy and apoptosis, implicated by differential expression of p53A and p53B under oxidative stress (Robin et al. 2019).

Beyond the conserved role in regulating apoptosis upon DNA damage, p53 controls tissue and metabolic homeostasis. Under nutrient deprivation, *p53* null mutant flies exhibit reduced survival, highlighting its role in coordinating metabolism and nutrient consumption (Barrio et al. 2014). *p53* also regulates growth and proliferation in a coordinated, non-autonomous manner and modulates apoptosis in response to stress, such as rRNA depletion (Mesquita et al. 2010). Furthermore, p53 is necessary to maintain imaginal disc plasticity and regenerative potential (Wells and Johnston 2012) and to act

as a general sensor of competitive confrontation during MYC-induced cell competition (de la Cova et al. 2014). Notably, p53 isoforms have not been assessed in these experiments despite growing evidence that their function can differ significantly depending on the cellular context in which they are expressed. Thus, it may be important to consider that distinct signals and tissue-specific expression programs could drive isoform-specific roles in stress response and gene regulation.

While the isoform-specific roles of p53A and p53B have been increasingly elucidated in the context of DNA damage induced by ionizing radiation (Chakravarti et al. 2022; Zhang et al. 2015), much less is known about how individual isoforms, including the less characterized p53C, are differentially regulated in response to nucleolar stress. To further understand this, we designed primers with enhanced specificity for individual p53 isoforms. Our study aimed to compare the upregulation of these isoforms following the downregulation of the nucleolar protein NOC1, which we have previously shown to cause nucleolar disruption, impair ribosome biogenesis, and induce DNA damage, resulting in the upregulation of p53 both in flies and in human cells (Pederzolli et al. 2025; Destefanis et al. 2022; Rambaldelli et al. 2025).

Our data identify that the specific *p53B* and *p53C* isoforms are upregulated upon NOC1 reduction and may function as key regulators in response to nucleolar perturbation. In contrast**,** *p53A* expression remains largely unchanged, indicating a response distinct from the genotoxic stress response, where p53A is predominantly expressed. These results point to isoform-specific roles in nucleolar stress signaling. Additionally, our findings suggest potential autoregulatory interactions among p53 isoforms, where the induction of one may influence the transcription or stability of others. Together, these data underscore the importance of characterizing isoform-specific p53 functions to better understand the complexity and evolutionary conservation of cellular stress responses. Moreover, our work provides novel molecular tools and insights into the isoform-specific regulation of p53 in *Drosophila*, offering the possibility to analyze which distinct *p53* isoforms are engaged in the stress pathways network.

Materials and Methods

Drosophila husbandry and lines

Animals were raised at low density in vials containing standard fly food, composed of 9 g/l agar, 75 g/l corn flour, 50 g/l fresh yeast, 30 g/l yeast extract, 50 g/l white sugar, and 30 ml/l molasses, along with nipagine (in ethanol) and propionic acid. The crosses and flies used for the experiments are kept at 25°C, unless otherwise stated. Line used: w^{1118} from VDRC #6000, *Rotund* > Gal4 BDRC#76179, UAS-NOC1-RNAi BDRC #25992, $p53^{5A-1-4}$BDRC #6815, $p53^{A2.3}$ and $p53^{B41.5}$ from C. Estella (Centro de Biología Molecular Severo Ochoa, Madrid, Spain).

Alkaline Comet Assay

In *Drosophila,* gene expression, whether ubiquitous or tissue-specific, is commonly achieved using the *UAS-Gal4* system, where a specific tissue-promoter drives Gal4 expression to activate a gene of interest, cloned under the UAS sequences (Brand and Perrimon 1993) Since ubiquitous downregulation of NOC1 impairs animal growth (Destefanis et al. 2022), and compartment-specific knockdown is unsuitable for our experiments, as we require dissection and analysis of cells from the entire imaginal disc to obtain a homogeneous population with the same genotype for the comet assay. To address this, we employed a temporally controlled expression system using the *Actin-Gal4* driver in combination with the temperature-sensitive *Gal80-ts* allele (Germani et al. 2018). At the permissive temperature of 18 °C, *Gal80-ts* inhibits Gal4 activity. When the temperature is shifted to 30 °C, *Gal80-ts* becomes inactive, allowing Gal4 to drive expression of the *UAS-NOC1-RNAi* construct. This approach allowed us to circumvent the small size observed in *Actin>Gal4; UAS-NOC1-RNAi* animals. Temporal knockdown of *NOC1* was initiated five days after egg laying (AEL), when larvae had reached the second instar stage at the permissive temperature of 18 °C. The animals were then shifted to 30 °C for 60 hours, during which Gal4 was active and induced ubiquitous expression of *NOC1-RNAi*. Wing imaginal discs were dissected and incubated in Ringer's solution,

then enzymatically digested with Collagenase in TrypLE at 37–38 °C for 30 minutes. Tissues were dissociated by pipetting, neutralized with FBS, filtered through a 40 µm mesh, and centrifuged. Cells were washed with PBS, viability assessed with Trypan Blue, and mixed with low-melting-point agarose. The mixture was placed on agarose-coated slides, solidified at 4 °C, and coverslips removed. Slides were lysed in a cold buffer, incubated in an alkaline solution, and subjected to electrophoresis. After neutralization and Hoechst staining, photos of nuclei were imaged using a Zeiss Axio Imager fluorescent microscope with a 40X objective, and DNA damage was analyzed with CometScore 2.0. For a detailed protocol, see (Pederzolli et al. 2025).

RNA Extraction and RT-qPCR

RNA extraction was performed with the RNeasy Mini Kit (Qiagen). Five larvae or 30 wing discs were collected and placed in 250µl of lysis buffer, then processed following the manufacturer's instructions. The isolated RNA was quantified with the Nanodrop (Thermo Scientific) and stored at -80 °C for long periods. RNA (1µg) was retro-transcribed into cDNA using the SuperScript IV VILO Master Mix (Invitrogen) To perform retro-transcription, the mix was incubated at 25°C for 10 minutes, 50°C for 10 minutes, and 85°C for 5 minutes. The obtained cDNA was used to perform qPCR with the SYBR Green PCR Kit (Qiagen). The final mix for each sample to be tested was composed by 8µl of cDNA, 2µl of primers (10µM), and 10µl of SYBR Green reaction mix. Reactions were carried out by a BioRad CFX96 machine with the following protocol: 50°C for 2 minutes, 95°C for 2 minutes, 95°C for 15 seconds and 60°C for 30 seconds (repeated for 45 cycles), 72°C for 1 minute. Analyses were done using Bio-Rad CFX Manager software. The relative abundance level for each transcript was calculated using the $2^{-\Delta\Delta Ct}$ method, normalizing on the expression of *actin5C* and then normalized to the control sample. Experiments comprise at least three independent biological samples and with two replicates each point. The sequences of the primers used are in Table 1.

Dissections and immunofluorescence

Larvae were collected at the third-instar stage, dissected in 1× phosphate-buffered saline (PBS), and fixed for 30 min in 4% paraformaldehyde (PFA) at room temperature (RT). After 15 minutes of tissue permeabilization with 0.3% Triton X-100, samples were washed in PBS with 0.04% Tween 20 (PBS-T) and blocked in 1% bovine serum albumin (BSA) for 1 hour at RT. Samples were incubated overnight at 4°C with primary antibodies in 1% BSA and, after washing, with Alexa-Fluor-488- or 555-conjugated secondary antibodies in BSA. During washing in PBS-T, nuclei were stained with Hoechst 33342 (Thermo Fisher Scientific). Imaginal discs were dissected from the carcasses and mounted on slides with Vectashield (LsBio-Vector Laboratories). Images were acquired using a Leica SP8 confocal microscope or Zeiss Axio Imager fluorescent microscope (stated in each figure legend) and analyzed with the Fiji program to measure fluorescence. Images were assembled using Photoshop (Adobe). Primary antibodies used were rabbit anti-cleaved Caspase3, 1:400 (Cell Signaling 9661); mouse anti-p53, 1:250 (DSHB #25f4).

Image processing

Raw confocal images were processed with Fiji to obtain a z-stack projection (using Average Intensity or Max Intensity options), then all the images coming from the same experiment were processed, enhancing the brightness of all the channels equally for all the images.

Western Blots

Proteins were extracted from 10 third-instar larvae and collected in 250 µl of lysis buffer (50 mM HEPES pH 7.4, 250 mM NaCl, 1 mM EDTA, and 1.5% Triton X-100) containing phosphatase and protease inhibitors (Roche). Samples were run on a 10% SDS-polyacrylamide gel and then transferred to a nitrocellulose membrane. After Ponceau staining, the membrane was blocked with 5% non-fat milk in TBS-T. Then the membranes were incubated with primary antibody mouse anti-p53 (1:200, Dmp53 H3, DSHB), and

mouse anti-actin (1:1000; DSHB 224-236-1), followed by incubation with HRP-conjugated secondary antibodies (Santa Cruz Biotechnology). The signal was detected using ECL LiteAblot Plus (Euroclone) and the UVITec Alliance LD2. Since p53 and actin have similar weights, the membrane was stripped with a harsh stripping solution (2% Sodium dodecyl sulfate, Tris-HCl 64mM, and βmercaptoethanol 100mM) at room temperature for 30 minutes. Then, after several washings with TBS-T, the membrane was re-blocked for 1 hour at room temperature with 5% non-fat milk in TBS-T and incubated with primary and secondary antibodies as described above.

Results

1.1 Reduction of nucleolar NOC1 induces DNA damage, apoptosis and p53 upregulation.

We previously demonstrated that downregulation of the nucleolar factor NOC1 in *Drosophila* tissues leads to defects in the rRNA processing (Destefanis et al. 2022). Specifically, downregulation of *NOC1* in cells of the wing imaginal discs, using the *rotund* promoter, is associated with DNA damage as evidenced by the comet-like morphology of the nuclei in NOC1-RNAi cells (Figure 1A-B, and (Pederzolli et al. 2025). These nuclei show a statistically significant increase in the comet tail length (or tail moment, calculated as tail length multiplied by the percentage of DNA in the comet head), indicating the presence of double-strand breaks and DNA damage (Figure 1C), a feature absent in the nuclei of wild-type w^{1118} cells. Notably, the reduction of *NOC1* is accompanied by a significant increase in apoptosis, visible by Caspase3 staining in cells of the wing pouch (Figure 1D-E). Additionally, we observed an upregulation of p53 at both the transcription and protein levels in the wing pouch (Figure 1E-F). Together, these findings are consistent with a cellular response to nucleolar stress induced by impaired rRNA processing in cells with reduced NOC1 function. Based on this data, we decided to design isoform-specific qPCR primers to analyze how individual p53 isoforms respond to NOC1 knockdown.

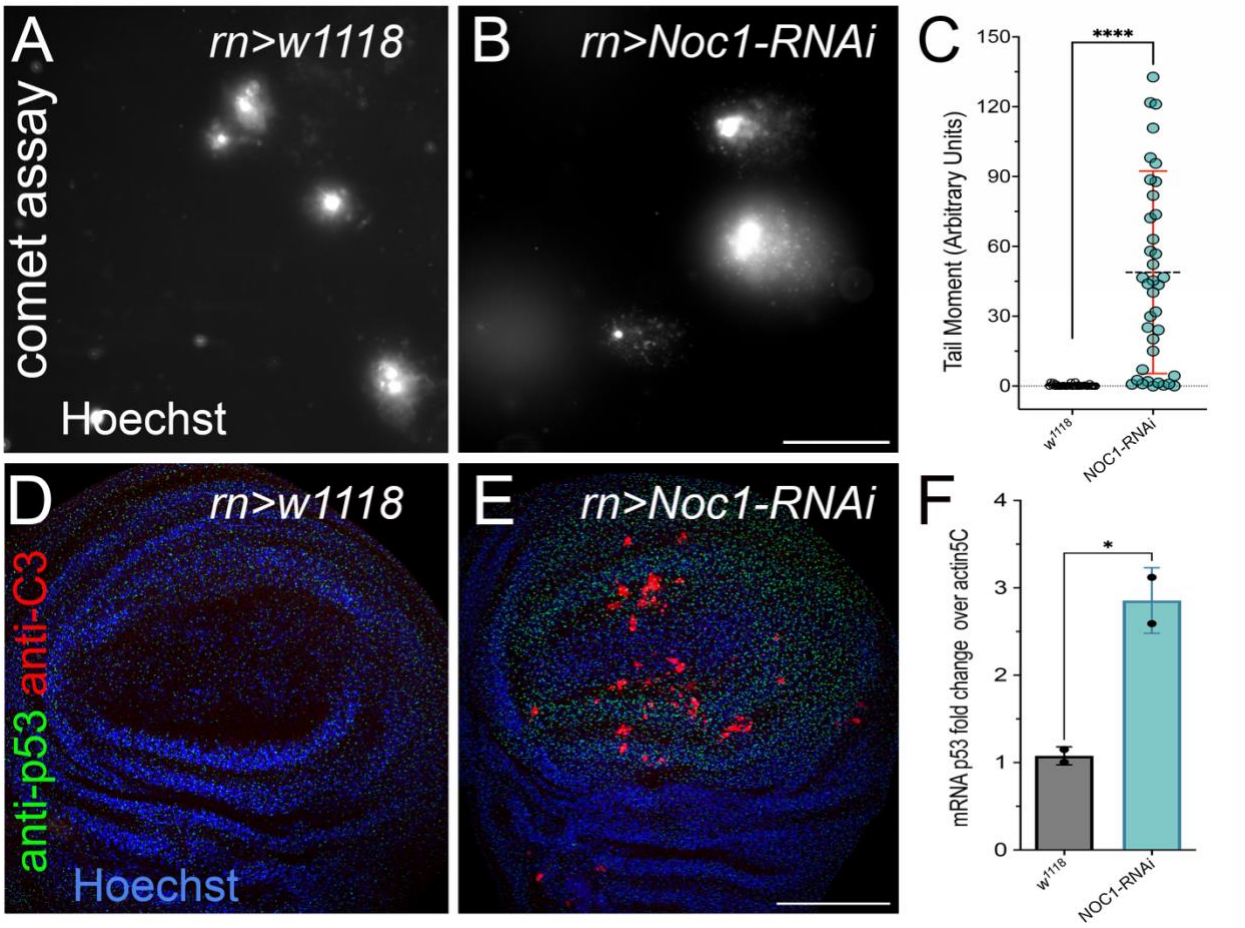

Figure 1. NOC1 Downregulation Causes DNA Damage and p53 Upregulation

(A-C) Comet assay showing fluorescent images of nuclei stained with Hoechst (white) from cells of the wing imaginal discs from w^{1118} third instar larvae (A), and from animals where *NOC1* was temporarily reduced for 60 hours using the *Act-Gal80*^{ts} allele. (B), scale bar is 50μm. (C) Quantification of single-cell tail moment from comet assay performed on nuclei from the genotypes shown in A and B. Statistical analysis was calculated using the non-parametric Kruskal-Wallis as in (Pederzolli et al. 2025). (D-E) Confocal images of wing imaginal discs from third instar w^{1118} larvae (D), or from the same stage animals with reduced *NOC1* expression in the wing pouch using the *rotund* (*rn*) promoter (E). Tissues were immunostained for the expression of p53 (green) and for Caspase3, as a marker of apoptosis (red). Nuclei were stained with Hoechst (blue). Scale bar is 100μm. (F) qPCRs from RNA extracted from wing imaginal discs from w^{1118} animals or with reduced *NOC1* using the *rn* promoter. p53 upregulation was analyzed using p53 pan isoform primers

(Table 1). In C, the asterisks represent the *p-values* from Student's *t*-test in one out of three independent experiments performed, where the dots represent the numbers of nuclei analyzed. In F, the dots represent the number of independent biological replicates. * = $p < 0.05$ and **** = $p < 0.0001$, and the error bars indicate the standard deviations.

1.2 p53 locus and novel primers for detecting distinct p53 isoforms

The *Drosophila* genome contains a single *p53* locus (Figure 2A, FBgn0039044 and gene ID:2768677) on chromosome 3R that produces four distinct transcripts through alternative promoter usage and splicing, resulting in four isoforms (Figure 2B). The canonical *p53A* (also referred to as ΔNp53) lacks part of the N-terminal Transactivation Domain (TAD), producing a protein of approximately 44 kDa. The *p53B*, retains the full TAD, resulting in a larger protein of about 56 kDa, while the remainder of the sequence is identical to that of *p53A*. p53C shares the same amino acid sequence as p53A but originates from an alternative transcription start site, producing a longer transcript. Finally, *p53E* is the shortest isoform and completely lacks the TAD at the N-terminus; it is thought to function as a dominant-negative regulator of the other three isoforms.

Although primers have been published to distinguish between *p53* isoforms, none have been fully optimized to reliably differentiate between *p53A* and *p53B* isoforms. Furthermore, primers specifically distinguishing *p53B* from *p53C*, or exclusively targeting *p53C*, are currently unavailable. Therefore, we designed and optimized a new set of primers to enable accurate isoform-specific analysis (Table 1).

Target	Sequence	Note
p53A/C	F: TATATCACAGCCAATGTCGTG	This work
	R: CCTCCGTGGAGTCATCC	
p53B	F: CCACAAGGGCACTGATTC	This work
	R: ATTCCGATCCCGATACCTC	
p53C	F: GTGAGCAAATTCAAAACACGC	This work
	R: CCATTCGCCACGCAG	

p53 pan isoform	F: CCAAGCTAGAGAATCACAACATCG	(Zhang et al. 2015)
	R: TCGAGTACATCCAAAGAGACTTGG	
p53A	F: CCAACAAGATCGCTTGATCAGATA	(Zhang et al. 2015)
	R: CCACGACATTGGCTGTGATA	
p53B	F: AACATGATGCAGTTCACGAACAA	(Zhang et al. 2015)
	R: TGTTATTGCCATCGGAATTATTG	

Table 1: Sequences of the primers originate in this work and previously published

To ensure isoform specificity and accurate validation, primers were designed using the sequences of the available *p53*$^{A5.1.4}$ null lines and the isoform-specific *p53A* and *p53B* mutant lines. Briefly, the *p53A* null line carries a 23bp deletion and 7bp insertion at the end of the first exon which expands also in the first intron (Robin et al. 2019); the mutant *p53B* null line has a 14 bp deletion and 1 bp insertion in the second exon, resulting in multiple early STOP codons (Chakravarti et al. 2022); and the *p53*$^{A5.1.4}$ null line carries a large deletion of approximately 3.3 Kb that removes four exons, preventing the transcription of a functioning mRNA resulting in a complete loss of p53 protein expression (Figure 2C) (Rong et al. 2002).

The new primers for the *p53A* isoform span the exon-exon junction between exons 1 and 2 (Figure 2D-i, shown as light green arrows in the panel, and Table1), providing enhanced specificity compared to earlier designs (shown as arrows in pink, and Table 1). Like the previously available primers, this set can be used to assess *p53A* expression in the p53A null line as the forward primer anneals upstream of the deleted region, while the reverse primer anneals right after the deletion, allowing the amplification of a specific region of the mutant (Figure 2D-ii). A limitation of the new primers, as with previously published ones, is their inability to distinguish between *p53A* and *p53C* isoforms. This overlap is, unfortunately, unavoidable due to the high sequence similarity between the two isoforms. To design distinct primers for each *p53B* and *p53C* isoform, we took advantage of the difference in the length of their 5′ untranslated region (5'UTR) between the two isoforms (Figure 2E). While the reverse primer anneals in a common sequence between *p53B* and

p53C, the forward primer for *p53B* anneals at the end of the second exon and finishes at the beginning of the third one (green arrows in Figure 2E-i and 2E-iii). This allows for maximum specificity, ensuring the capture of only *p53B*. This set of primers is good for screening *p53B* in *p53B* null lines, as they do not anneal in the deleted part (Figure 2E-ii).

Through detailed analysis of the 5′UTR sequence of *p53C*, we identified a region unique to this isoform (highlighted in orange in Figure 2F). Thus, we designed primers targeting this specific region, allowing selective detection of *p53C*, providing a unique primer set for this isoform.
Moreover, having *p53C*-specific primers enables more accurate interpretation of the signal from the *p53A* set of primers, which does not distinguish between the *p53A* and *p53C* isoforms.

Primer specificity was tested by performing qPCRs on RNA extracted from imaginal discs from w^{1118} third instar larvae. All primers amplify a single product, as evidenced by a single band observed in the gel (Figure 2G) and confirmed by their melting curve analysis, which shows a distinct peak for each primer (Supplementary Figure 1).

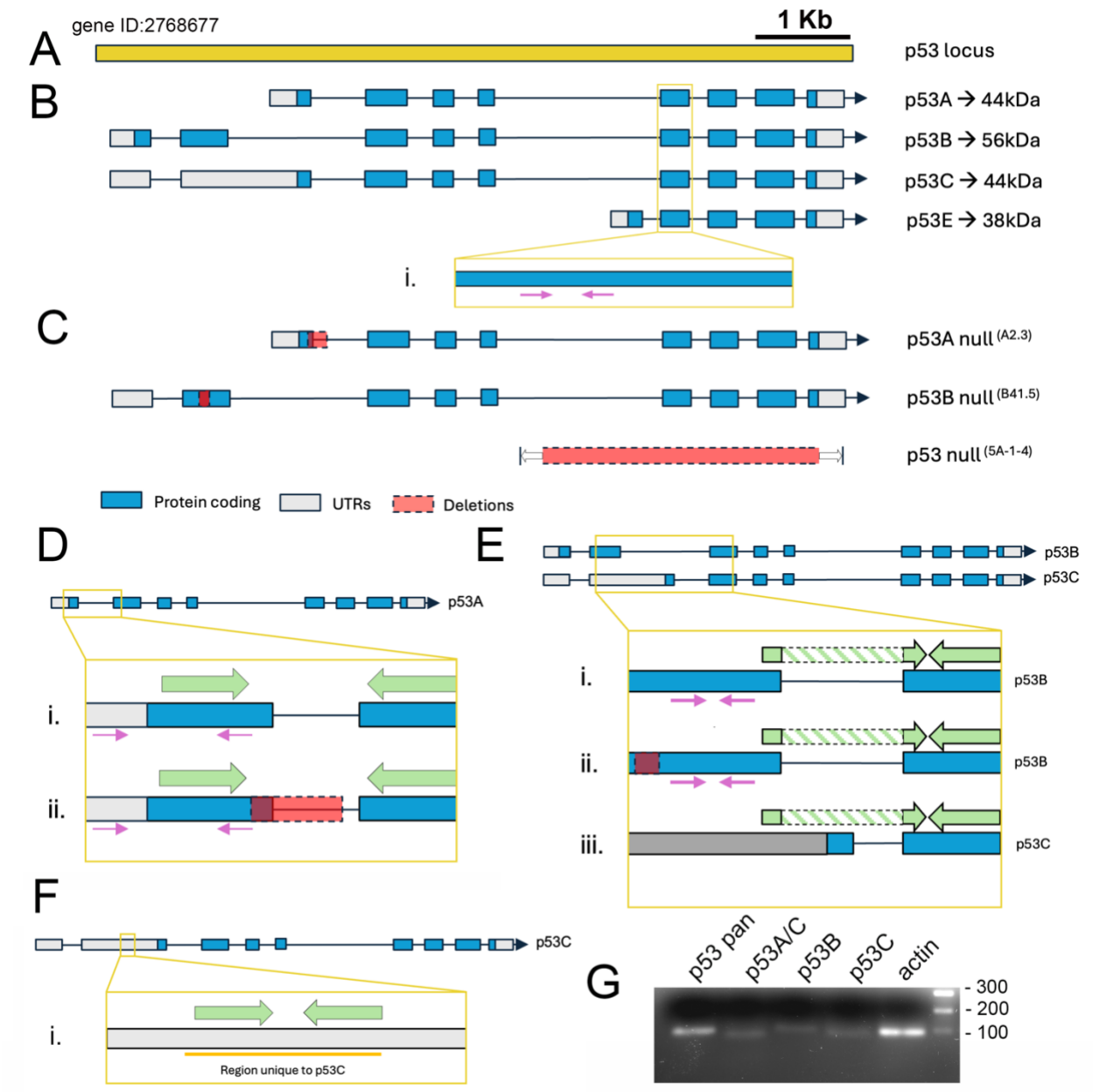

Figure 2. Schematic primer design and p53 locus used to detect specific isoforms. (A-B) Schematic representation of the *p53* locus (gene ID 2768677) and of the p53 isoforms *A, B, C,* and *E*. (B-i), magnification of a common exon with the representation of the region where the primers that capture all *p53* isoforms anneal (Zhang et al. 2015). These primers were used in Figure 1F and will be referred to as "p53 pan". (C) Schematic representation of the *p53A*$^{A2.3}$, *p53B*$^{41.5}$, and *p53*$^{A5.1.4}$ null mutant alleles. *p53A*$^{A2.3}$ null line was generated with a deletion of 23bp deletion, and a 7bp insertion spanning from the end of the first exon until the first base of the first intron (in red), generating multiple early

STOP codons (Supplementary Figure 2). This deletion also affects the *p53C* isoform, leading to no production of p53C protein, according to Chakraborty et al. 2022. *p53B*$^{41.5}$ null line was generated with a 14bp deletion and a 1bp insertion in the second exon that causes a frameshift and introduces premature stop codons (Supplementary Figure 2). *p53*$^{A5.1.4}$ null line has a deletion of 3.3 kb, removing the common 3' coding region (in red). (D) *p53A* isoform. (D-i and ii), magnification of exons 1 and 2 of *p53A* and *p53A*$^{A2.3}$ null isoform, respectively, displaying where the primers designed in this study anneal (in green) and compared to previous primers (in pink). As shown in D-ii, the new primers can also be used to identify *p53A* in the *p53A*$^{A2.3}$ null mutant, as the forward primer does not anneal within the deleted region. Conversely, 1 bp of the previous reverse primer (pink) mismatch in the *p53A* null line. Note that this new set of primers can also capture *p53C* isoform; therefore, they will be referred to as "p53A/C". (E) *p53B* and *p53C* isoforms. (E-i, ii, and iii), magnification of exons 2 and 3, which are common to both isoforms, showing where the primers designed in this study anneal (in green). Note that the new pair can distinctly capture the *p53B* isoform, while the old primers (in pink) also capture *p53C*. Moreover, the new pair is also suitable for studying the *p53B* null line since the forward primer does not anneal in the deleted region marked in red (E-ii). This pair of primers will be referred to as "p53B". (F) *p53C* isoform. (F-i), magnification of the region in exon 2 showing the sequence of 78 bp, from 440 to 518 nucleotides from the beginning of the p53C transcript (in orange), present only in this isoform. Optimized primers for the detection of this isoform are represented in green. This new set of primers will be referred to as "p53C". (G) Photo of a 2% agarose gel showing qPCR amplified products from RNA extracted from wing imaginal discs from *w*^{1118} third instar larvae using the indicated primers and *actin* as a control. A single band is visible for each primer pair, indicating the specificity of the new optimized primers.

1.3 Validation of isoform-specific primers in wild-type and p53 mutant backgrounds.

To further assess the specificity and to complete the characterization of the newly designed primer sets, we conducted qPCR analysis on RNA from wild-type control w^{1118} and *p53* mutant lines using primers targeting the single *p53* isoforms (Table 1).
As shown in Figure 3A, the p53 pan primers, which target a region common to all the *p53* isoforms (Figure 3-i), detect p53 transcript levels in the *p53A* null line that are comparable to those of control w^{1118}. In contrast, the *p53B* null line exhibits a significant increase in p53 expression, suggesting a potential compensatory upregulation of the other isoforms in response to the loss of *p53B.*

Using the p53A/C primers, we observed that the p53A/C isoform levels were reduced by approximately 50% in the *p53A* null line; however, this reduction was not statistically significant (Figure 3B). In contrast, the *p53B* null line showed a significant 2-fold increase in *p53A/C* expression. Like the data in Figure 3A, these data suggest the presence of a compensatory response to the other isoforms when *p53B* is eliminated in null animals, while loss of *p53A* has minimal effect on overall transcript abundance.

Analysis of *p53B* mRNA expression unexpectedly shows significant upregulation in the p53B null line (Figure 3C). Since the mutation does not prevent transcription and the primers likely target regions downstream of the deletion, the mutant mRNA can still be detected by qPCR; moreover, it suggests the existence of a compensatory or autoregulatory feedback mechanism that modulates *p53B* expression in response to its absence.

Finally, analysis on *p53C* isoform, using primers that specifically detect these transcripts, reveals a significant reduction in its expression in both *p53A* and *p53B* null lines, which is about 80% and 40 % respectively (Figure 3D). These data suggest that both *p53A* and *p53B* isoforms, directly or indirectly, participate in the regulation or stability of *p53C* expression. Importantly, the complete absence of *p53A/C*, *p53B*, *p53A,* or *p53C* transcript

in the *p53*$^{A5.1.4}$ null line confirms the specificity and reliability of the isoform-targeted primer set used in this study.

To complement the transcript-level analysis and analyze isoform-specific p53 protein expression, Western blot analysis was performed to visualize p53 expression across different p53 mutant backgrounds, using an anti-p53-H3 antibody that was raised against the full-length p53A protein (Ollmann et al. 2000). As expected, p53 expression was absent in *p53* null animals (Figure 3E). In *p53A* null background, a modest reduction in its expression, relative to *w*^{1118}, was observed. This decrease is consistent with the qPCR results (Figure 3B). Conversely, extracts from *p53B* null animals show a substantial increase in overall p53 protein levels, supporting the qPCR finding of elevated *p53A/C* expression in the absence of p53B. Due to the lack of isoform-specific antibodies for p53A or p53C proteins, we cannot determine which isoform is upregulated in this context.

In addition, the p53B isoform, which has the predicted molecular weight of 56 KDa, was not detected in any genotype, likely due to its much lower abundance relative to the other isoforms (Zhang et al. 2015).

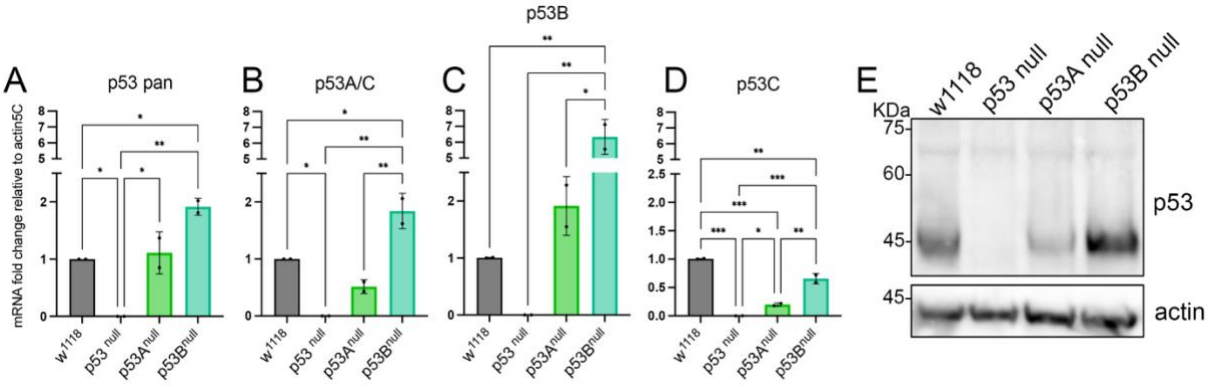

Figure 3. RT-qPCR characterization of p53 mutant lines using isoform-specific primers. qPCRs showing specific mRNA changes in RNAs extracted from whole third instar larvae of the annotated *p53* mutant lines. (A) p53 pan recognizes all *p53* isoforms. (B) p53A/C recognizes specifically only *p53A* and *p53C* isoforms. (C) p53B recognizes only the relative isoform. (D) p53C recognizes only the relative isoform. Expression levels were normalized to *actin-5C* and compared to the levels in control *w*^{1118} animals. RNA

was extracted from five whole larvae of the respective genotype. The asterisks represent the *p*-values from One-way analysis of variance (ANOVA) with Tukey multiple comparison: * = $p < 0.05$, ** = $p < 0.01$, and *** = $p < 0.001$, and the error bars indicate the standard deviations. (E) Western blot analysis from larval extracts showing the relative amount of p53 protein from w^{1118} animals or different p53 mutant isoforms. Actin was used as the loading control. The band visible between 60 and 75 kDa is a non-specific signal present in all lanes.

1.4 p53B and p53C are the predominantly upregulated isoforms in NOC1 downregulated cells.

Our initial assessment for *p53* mRNA expression in cells with reduced *NOC1* amplifies a conserved region present in all four *p53* isoforms, as illustrated in the magnified view (Figure 2B-i). Considering that *NOC1* reduction leads to rRNA accumulation and increased p53 levels (Figure 1B-C), both hallmark features indicative of nucleolar stress, and given the distinct and sometimes opposite roles of p53 isoforms under different stress conditions, we decided to analyze isoform-specific *p53* responses upon *NOC1-RNAi*.
As shown in Figure 4A, analysis of *p53* expression in cells of the wing imaginal discs from animals with reduced NOC1 revealed a significant upregulation of *p53* using the p53 pan isoform primers (Figure 4A and Figure 1F). Isoform-specific primer analysis revealed a striking 4-fold upregulation of the *p53B* isoform in *NOC1-RNAi* wing disc-cells (Figure 4A). Notably, *p53C* expression was similarly upregulated *to p53B* in *NOC1-RNAi* cells, as detected using the newly designed *p53C*-specific primers. In contrast, *p53A* displayed only a modest and not significant increase. These findings lead us to conclude that *p53B* and *p53C* may play a more prominent role in the cellular stress response associated with impaired ribosome biogenesis and nucleolar stress.

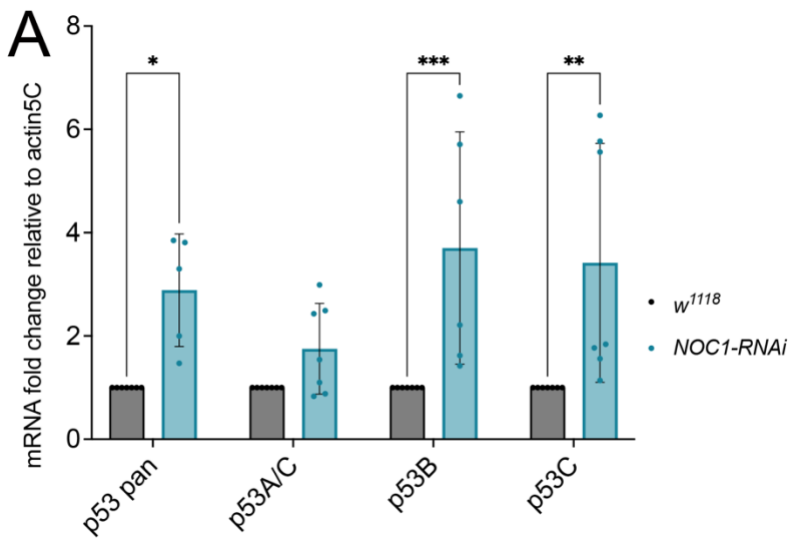

Figure 4 p53B and p53C are upregulated in NOC1 downregulated cells.

(A) qPCRs from RNA extracted from wing imaginal discs of w^{1118} animals and expressing *NOC1-RNAi* in the wing pouch using the *rotund* promoter. Data are expressed as fold of mRNA expression change over *actin5C*, used as a control for normalization. The asterisks represent the *p*-values from One-way analysis of variance (ANOVA) with Tukey multiple comparison: * = $p < 0.05$, ** = $p < 0.01$, and *** = $p < 0.001$, and the error bars indicate the standard deviations. Data represent three independent experiments, with each sample for each genotype consisting of a pool of 30-40 wing imaginal discs.

Discussion:

Previous primer designs have played a crucial role in advancing our understanding of p53 in biology and have provided essential tools for characterizing their function. Taking advantage of these functional efforts, our updated primer set offers enhanced resolution, particularly in contexts where overlapping exon usage or alternative transcription start sites make isoform discrimination more challenging.

In this study, we present an optimized and validated set of isoform-specific primers designed for the accurate detection and quantification of *Drosophila* p53 transcript variants (Table 1).

We took advantage of the available p53 mutant lines to validate primer specificity and, in parallel, to reassess that in the *p53*$^{5A-1-4}$ null allele, also referred to as *p53* null, the *p53A/C*, *p53B,* and *p53C* isoforms are undetectable. In contrast, analysis of the *p53A* and *p53B* mutant lines revealed possible novel trends in the regulatory network that modulates p53 isoforms.

These analyses show that the *p53A* null line retains approximately 20% of both *p53A* and *p53C* transcript levels (Figure 3B and D). In parallel, western blot analysis, using a pan-p53 antibody (Ollmann et al. 2000), reveals a 50% reduction in total p53 protein, compared to that from wild-type *w*^{1118}, with a prominent 44 kDa band. Given that the p53B isoform has a higher molecular weight of 56 KDa, the visible 44KDa signal most likely corresponds to residual p53C protein. This interpretation aligns with the relatively low transcript level of *p53C* detected (Figure 3D) and suggests incomplete ablation of these isoforms in the *p53A* null animals, underscoring the importance of precise transcript-level validation.

Conversely, the *p53B* null mutant exhibited a notable upregulation of *p53A* transcripts (Figure 3C), which is represented in the western blot by the increase of the 44 KDa protein in the p53B null lane (Figure 3E). This likely reflects a compensatory mechanism triggered by the functional loss of p53B. Indeed, despite the introduction of premature stop codons within the coding sequence of the *p53B* mutant (Supplementary Figure 2), our qPCR analysis revealed an upregulation of the corresponding mRNA, whereas no detectable protein was observed by western blot (Figure 3E), indicating that transcription proceeds but translation is abrogated, likely due to nonsense-mediated decay or ribosomal stalling.

Taken together, these data may suggest the presence of a compensatory or autoregulatory feedback mechanism that modulates *p53B* expression in response to its loss, potentially involving crosstalk with other *p53* isoforms or regulatory factors to maintain cellular homeostasis. In support of this possibility, we also observed a two-fold increase in *p53A* transcript levels in the *p53A* null line (Figure 3C), although this upregulation is not statistically significant.

These results highlight the added value of p53-isoform-specific primers in complementing existing genetic models of p53, enabling a more refined understanding of complex mutant phenotypes and their potential compensatory responses.

Our primers further allowed us to study isoform-specific expression of p53 in response to nucleolar stress, a condition induced by perturbation in ribosome biogenesis that activates a p53-dependent apoptotic response (Lindstrom et al. 2022). By specifically depleting NOC1, a critical factor for proper rRNA processing and ribosomal subunit assembly (Milkereit et al. 2001; Destefanis et al. 2022), in cells of the wing imaginal discs, we observed DNA damage and a robust increase in *p53* transcript and protein levels, resulting in caspase-dependent apoptosis (Figure 1). Notably, we found that this apoptotic response results from specific *p53B* and *p53C* upregulation. This provides the first direct evidence of a functional role for *p53C* in mediating the cellular response to nucleolar stress and reinforces the role of *p53B* isoform in stress-induced apoptosis. The ability to clearly distinguish and quantify these two isoforms offers a valuable tool for dissecting their individual contributions in physiological and stress response conditions.

Remarkably, our findings also reveal key mechanistic differences in p53 regulation between flies and humans. In vertebrates, p53 activation in response to nucleolar stress is primarily mediated at the post-translational level, through protein stabilization via inhibition of the E3 ubiquitin ligase MDM2 by ribosomal proteins (Lindstrom et al. 2022). In contrast, *Drosophila* lacks a clear MDM2 homolog with E3 ligase activity, suggesting an alternative regulatory mechanism. The gene *companion of reaper* (*Corp*) has been proposed as a structural and partial functional analog of mammalian MDM2. Corp binds p53 and negatively regulates its levels through a feedback loop, like MDM2; however, it lacks an E3 ligase domain and thus cannot mediate canonical p53 degradation (Chakraborty et al. 2015). These distinctions point to a divergence in the evolution of p53 regulatory circuits, where transcriptional control may play a more prominent role in flies. This difference emphasizes the evolutionary divergence in p53 regulation and raises important questions about whether isoform-specific transcriptional control might also serve as a stress adaptation mechanism in vertebrates, including humans.

Further supporting the evolutionary conservation of nucleolar stress responses, our data showed that downregulation of the human *NOC1* gene homolog, called *CEBPZ* (Rambaldelli et al. 2025), also activates p53 both transcriptionally and at the protein level, consistent with our finding in *Drosophila* (Destefanis et al. 2022). NOC1 functions as part of a conserved nucleolar heterodimeric complex with NOC2 and NOC3, which is essential for pre-rRNA processing and 60S ribosomal subunit assembly as demonstrated both in yeast and *Drosophila* (Milkereit et al. 2001; Destefanis et al. 2022). Our finding that NOC1 depletion triggers p53 upregulation in both flies and humans highlights the evolutionary conservation of nucleolar stress responses. This conserved activation underscores the broader relevance of nucleolar stress-induced p53 signaling and emphasizes the value of isoform-specific tools in dissecting the underlying regulatory mechanisms.

Due to its low expression levels and unclear involvement in apoptotic pathways, we did not include the *Drosophila* p53E isoform in our analysis. Although this truncated variant, characterized by a unique N-terminal domain, does not induce apoptosis (Zhang et al. 2015), its potential function as a dominant-negative regulator of p53 activity suggests that understanding its physiological role is important, especially considering the complexity of p53 isoform expression and regulation.

In conclusion, these newly developed primers represent a valuable resource for the *Drosophila* community, enabling improved resolution of p53 isoform expression. This tool facilitates refined analysis of isoform-specific functions and regulatory mechanisms in development, homeostasis, and stress responses. Our reanalysis of *p53* mutant lines reveals previously unrecognized residual activity and compensatory regulation, highlighting the complexity of p53 regulation. Finally, the identification of *p53C* as a novel player in nucleolar stress-induced apoptosis expands our understanding of p53 isoform-specific roles and supports a model wherein transcriptional regulation predominates over post-translational control in *Drosophila* p53 biology.

Data Availability Statement

All data are available in the published manuscript and its online Supplementary Files 1 and 2. These files include the melting curve of the primer sets used and the sequences of the *p53*$^{A2.3}$ and *p53B*$^{41.5}$ mutants used in this manuscript.

Acknowledgments

We thank the Bloomington Stock Center (NIH P40OD018537). Department CIBIO Core Facilities is supported by the European Regional Development Fund (FESR) 2021–2027. The input from members of the COST Action CA21154 TRANSLACORE, supported by COST (European Cooperation in Science and Technology and by the Dipartimento di Eccellenza 2023-2027, Legge 232/2016 project n 40613, funded by the MUR. This document includes language and clarity improvements made using ChatGPT (OpenAI).

Author contributions

AVC performed the experiments, conceived the study, and contributed to the writing of the manuscript. SB contributed to the final version of the manuscript. VM performed the experiments and analyzed the data. PB participated in its design, coordinated and supervised the team, and participated in the writing and editing of the final manuscript. All authors have read and agreed to the published version of the manuscript.

Conflict of Interest

No competing interests are declared.

Funder Information

No specific funds for this manuscript are declared.

Bibliography

Barrio, L., A. Dekanty, and M. Milan, 2014 MicroRNA-mediated regulation of Dp53 in the Drosophila fat body contributes to metabolic adaptation to nutrient deprivation. *Cell Rep* 8 (2):528-541.

Boley, N., M.H. Stoiber, B.W. Booth, K.H. Wan, R.A. Hoskins *et al.*, 2014 Genome-guided transcript assembly by integrative analysis of RNA sequence data. *Nat Biotechnol* 32 (4):341-346.

Boukoura, S., and D.H. Larsen, 2024 Nucleolar organization and ribosomal DNA stability in response to DNA damage. *Curr Opin Cell Biol* 89:102380.

Brand, A.H., and N. Perrimon, 1993 Targeted gene expression as a means of altering cell fates and generating dominant phenotypes. *Development* 118 (2):401-415.

Brodsky, M.H., W. Nordstrom, G. Tsang, E. Kwan, G.M. Rubin *et al.*, 2000 Drosophila p53 binds a damage response element at the reaper locus. *Cell* 101 (1):103-113.

Chakraborty, R., Y. Li, L. Zhou, and K.G. Golic, 2015 Corp Regulates P53 in Drosophila melanogaster via a Negative Feedback Loop. *PLoS Genet* 11 (7):e1005400.

Chakravarti, A., H.N. Thirimanne, S. Brown, and B.R. Calvi, 2022 Drosophila p53 isoforms have overlapping and distinct functions in germline genome integrity and oocyte quality control. *Elife* 11.

de la Cova, C., N. Senoo-Matsuda, M. Ziosi, D.C. Wu, P. Bellosta *et al.*, 2014 Supercompetitor Status of Drosophila Myc Cells Requires p53 as a Fitness Sensor to Reprogram Metabolism and Promote Viability. *Cell Metab*.

Destefanis, F., V. Manara, S. Santarelli, S. Zola, M. Brambilla *et al.*, 2022 Reduction of nucleolar NOC1 leads to the accumulation of pre-rRNAs and induces Xrp1, affecting growth and resulting in cell competition. *J Cell Sci* 135 (23).

Dichtel-Danjoy, M.L., D. Ma, P. Dourlen, G. Chatelain, F. Napoletano *et al.*, 2013 Drosophila p53 isoforms differentially regulate apoptosis and apoptosis-induced proliferation. *Cell Death Differ* 20 (1):108-116.

Fogarty, C.E., and A. Bergmann, 2017 Killers creating new life: caspases drive apoptosis-induced proliferation in tissue repair and disease. *Cell Death Differ* 24 (8):1390-1400.

Germani, F., C. Bergantinos, and L.A. Johnston, 2018 Mosaic Analysis in Drosophila. *Genetics* 208 (2):473-490.

Ingaramo, M.C., J.A. Sanchez, and A. Dekanty, 2018 Regulation and function of p53: A perspective from Drosophila studies. *Mech Dev* 154:82-90.

Lindstrom, M.S., J. Bartek, and A. Maya-Mendoza, 2022 p53 at the crossroad of DNA replication and ribosome biogenesis stress pathways. *Cell Death Differ* 29 (5):972-982.

Mesquita, D., A. Dekanty, and M. Milan, 2010 A dp53-dependent mechanism involved in coordinating tissue growth in Drosophila. *PLoS Biol* 8 (12):e1000566.

Milkereit, P., O. Gadal, A. Podtelejnikov, S. Trumtel, N. Gas *et al.*, 2001 Maturation and intranuclear transport of pre-ribosomes requires Noc proteins. *Cell* 105 (4):499-509.

Ollmann, M., L.M. Young, C.J. Di Como, F. Karim, M. Belvin *et al.*, 2000 Drosophila p53 is a structural and functional homolog of the tumor suppressor p53. *Cell* 101 (1):91-101.

Pederzolli, M., E. Barion, A. Valerio, A.V. Cuda, V. Manara *et al.*, 2025 Optimized protocol for single-cell isolation and alkaline comet assay to detect DNA damage in cells of Drosophila wing imaginal discs. *STAR Protoc* 6 (1):103590.

Rambaldelli, G., V. Manara, A. Vutera Cuda, G. Bertalot, M. Penzo *et al.*, 2025 From Flies to Humans: Conserved Roles of CEBPZ, NOC2L, and NOC3L in rRNA Processing and Tumorigenesis. *bioRxiv*.

Robin, M., A.R. Issa, C.C. Santos, F. Napoletano, C. Petitgas *et al.*, 2019 Drosophila p53 integrates the antagonism between autophagy and apoptosis in response to stress. *Autophagy* 15 (5):771-784.

Rong, Y.S., S.W. Titen, H.B. Xie, M.M. Golic, M. Bastiani *et al.*, 2002 Targeted mutagenesis by homologous recombination in D. melanogaster. *Genes Dev* 16 (12):1568-1581.

Wells, B.S., and L.A. Johnston, 2012 Maintenance of imaginal disc plasticity and regenerative potential in Drosophila by p53. *Dev Biol* 361 (2):263-276.

Wylie, A., A.E. Jones, S. Das, W.J. Lu, and J.M. Abrams, 2022 Distinct p53 isoforms code for opposing transcriptional outcomes. *Dev Cell* 57 (15):1833-1846 e1836.

Zhang, B., M. Rotelli, M. Dixon, and B.R. Calvi, 2015 The function of Drosophila p53 isoforms in apoptosis. *Cell Death Differ* 22 (12):2058-2067.